Supplementary Information for

Inhalable nanovesicles loaded with a STING agonist enhance CAR-T cell activity against solid tumors in the lung

Tianchuan Zhu [1,†], Yuchen Xiao [1,†], Zhenxing Chen [1], Hanxi Ding [1], Shoudeng Chen [2,*], Guanmin Jiang [3,*], Xi Huang [1,*]

[1] Center for Infection and Immunity, Guangdong Engineering Research Center of Molecular Imaging, The Fifth Affiliated Hospital of Sun Yat-sen University; Zhuhai, 519000, Guangdong, China.

[2] Guangdong Engineering Research Center of Molecular Imaging, The Fifth Affiliated Hospital of Sun Yat-sen University; Zhuhai, 519000, Guangdong, China.

[3] Department of Clinical laboratory, The Fifth Affiliated Hospital of Sun Yat-sen University, Zhuhai, Guangdong 519000, China

† These authors contributed equally: Tianchuan Zhu, Yuchen Xiao.

* Corresponding author: huangxi6@mail.sysu.edu.cn (X. Huang),

jianggm3@mail.sysu.edu.cn (GM. Jiang), chenshd5@mail.sysu.edu.cn (SD. Chen).

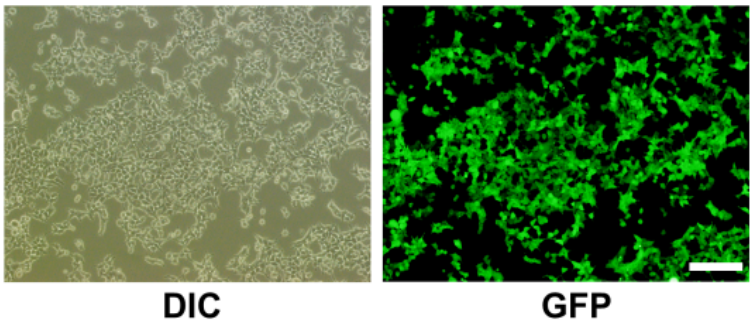

Supplementary Figure 1. Packaging of lentivirus encoding CAR protein. After the plasmid encoding CAR protein was co-transfected with the helper plasmid into 293T cells for 24 hours, the lentiviral packaging efficiency was reflected by fluorescence expression in 293T cells observed by inverted fluorescence microscopy. Experiment was repeated three times independently with similar results. Scale bar: 200 μm.

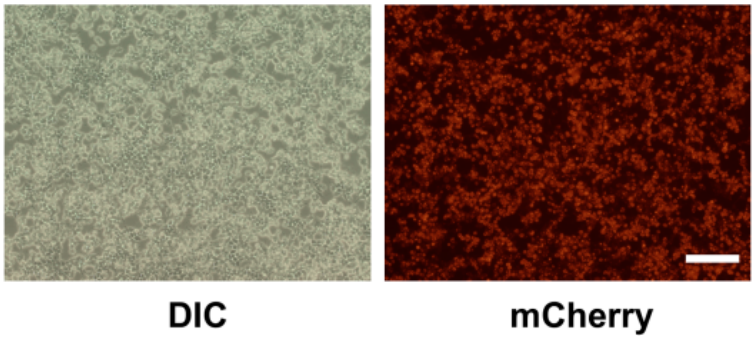

Supplementary Figure 2. Packaging of lentivirus encoding MSLN protein. After co-transfection of MSLN protein-encoding plasmid and helper plasmid into 293T cells for 24 hours, lentiviral packaging efficiency was reflected by fluorescence expression in 293T cells observed by inverted fluorescence microscopy. Experiment was repeated three times independently with similar results. Scale bar: 200 μm.

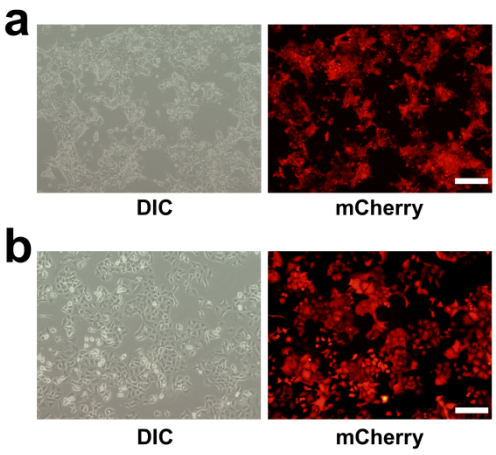

Supplementary Figure 3. Construction of LLC and B16 cells expressing MSLN. (a-b) The purity of (a) LLC-MSLN and (b) B16-MSLN cells was assessed by inverted fluorescence

microscopy after 2 weeks of screening of lentivirus-infected LLC and B16 cells with puromycin. Experiment was repeated three times independently with similar results. Scale bar: 200 μm.

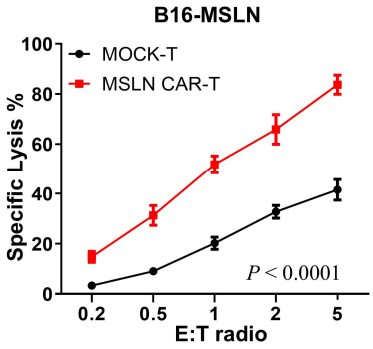

Supplementary Figure 4. Lysis rate of B16-MSLN cells by CAR-T cells. The lysis rate of CAR-T cells against B16-MSLN cells after co-incubation of CAR-T cells with B16-MSLN cells at effector-target ratios of 0.2, 0.5, 1, 2, and 5 for 24 hours was determined by LDH assay (n = 3 independent experiments). The p values were determined by two-way ANOVA with Tukey's post-test. Source data are provided as a Source Data file.

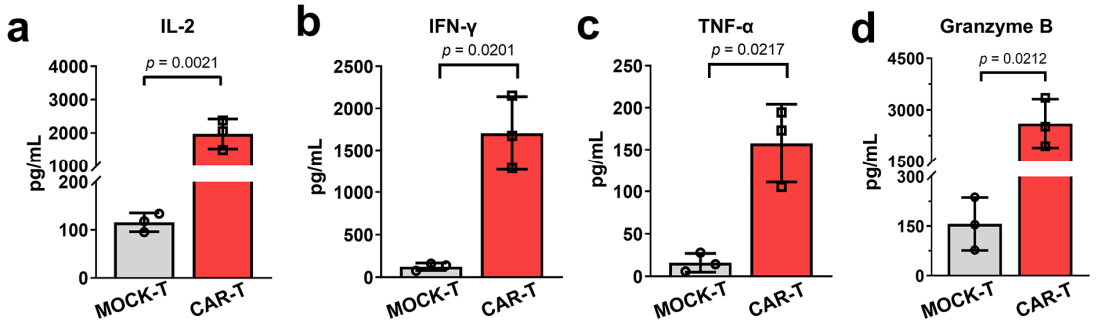

Supplementary Figure 5. Cytokine release upon lysis of B16-MSLN cells by CAR-T cells. The levels of cytokines IL-2, IFN-γ, TNF-α and granzyme B in the supernatants were determined by ELISA after co-incubation of CAR-T cells with B16-MSLN cells (n = 3 independent experiments). The p values were determined by Student's t test. Source data underlying a–d are provided as a Source Data file.

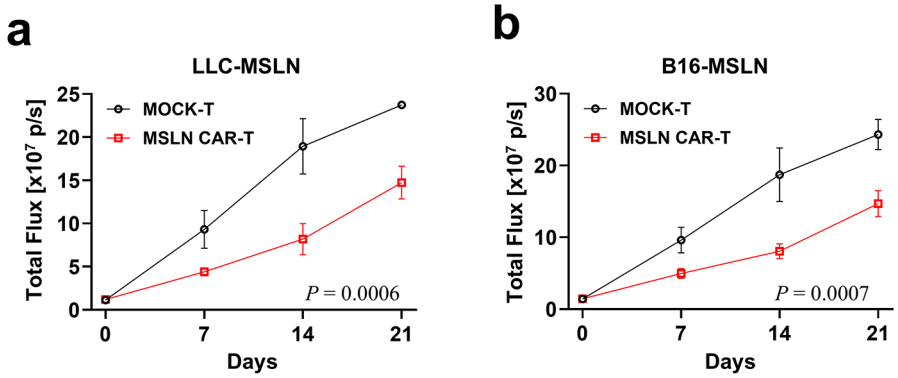

Supplementary Figure 6. Statistical analysis of bioluminescence intensity. Bioluminescence was measured by the IVIS system to evaluate tumor growth across different treatment groups, with statistical analysis of bioluminescence intensity ($n = 4$ mice). The p values were determined by two-way ANOVA with Tukey's post-test. Source data underlying a–b are provided as a Source Data file.

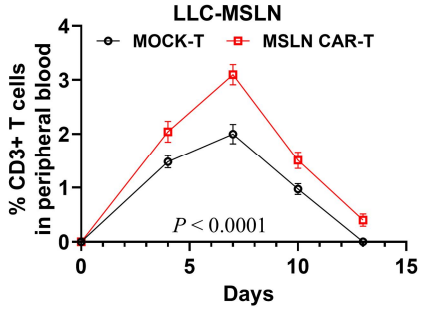

Supplementary Figure 7. Percentage of CAR-T cells in the peripheral blood of tumor-bearing mice. The percentage of CAR-T cells in peripheral blood at various time points after injection of GFP-expressing MOCK-T or MSLN CAR-T cells into LLC-MSLN tumor-bearing mice ($n = 4$ mice). The p values were determined by two-way ANOVA with Tukey's post-test. Source data are provided as a Source Data file.

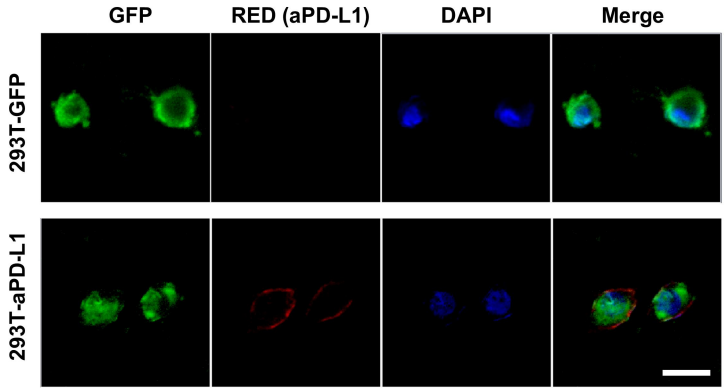

Supplementary Figure 8. Binding of 293-aPD-L1 cells to recombinant PD-L1 protein. After co-incubation of 293-aPD-L1 cells with recombinant PD-L1 protein, the cells were stained using an anti-PD-L1 antibody, and binding interactions were assessed *via* confocal microscopy. Experiment was repeated three times independently with similar results. Scale bar: 20 μm.

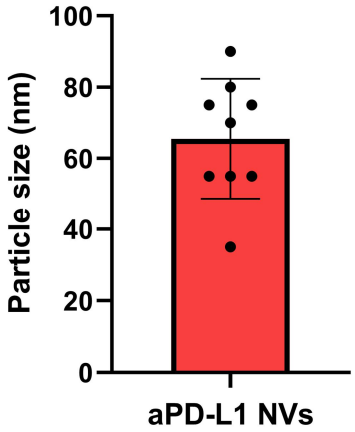

Supplementary Figure 9. Size distribution of aPD-L1 NVs. Statistical analysis of the size distribution of aPD-L1 NVs obtained through transmission electron microscopy ($n = 9$ nanovesicles). Source data are provided as a Source Data file.

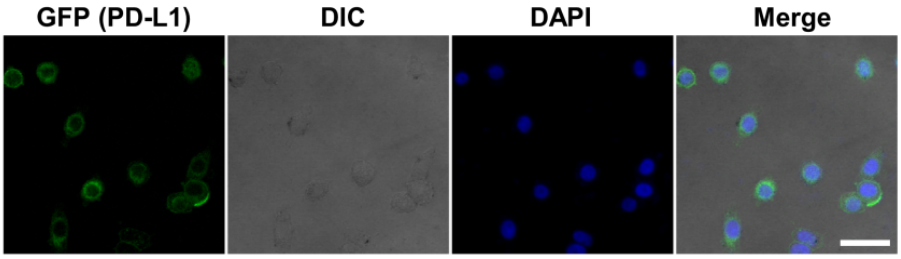

Supplementary Figure 10. Construction of PC-9 cells expressing GFP-PD-L1 in the membrane. After 2 weeks of screening lentivirus-infected PC-9 cells with puromycin, GFP expression on cell membranes was observed by confocal microscopy. Experiment was repeated three times independently with similar results. Scale bar: 50 μm.

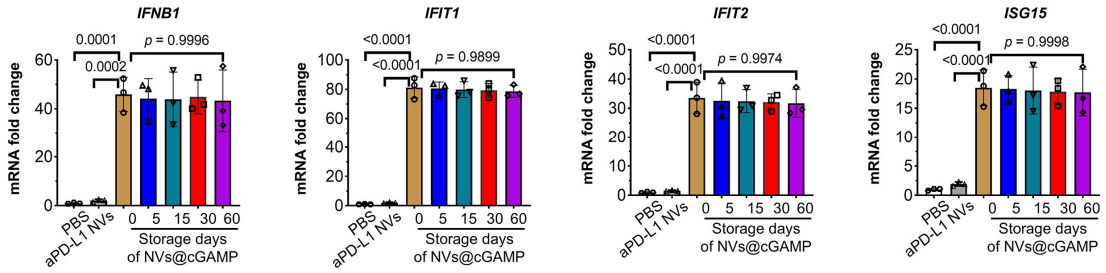

Supplementary Figure 11. Functional analysis of aPD-L1 NVs@cGAMP after storage. After storage of aPD-L1 NVs@cGAMP at -80°C for varying durations, co-culture with dendritic cells (DCs) resulted in altered mRNA expression levels of *IFNB1, IFIT1, IFIT2, and ISG15* in DCs. DCs treated with PBS and aPD-L1 NVs served as negative controls ($n = 3$ independent experiments). All data are expressed as mean ± S.D. The *p* values were determined by one-way ANOVA with Tukey's post-test. Source data are provided as a Source Data file.

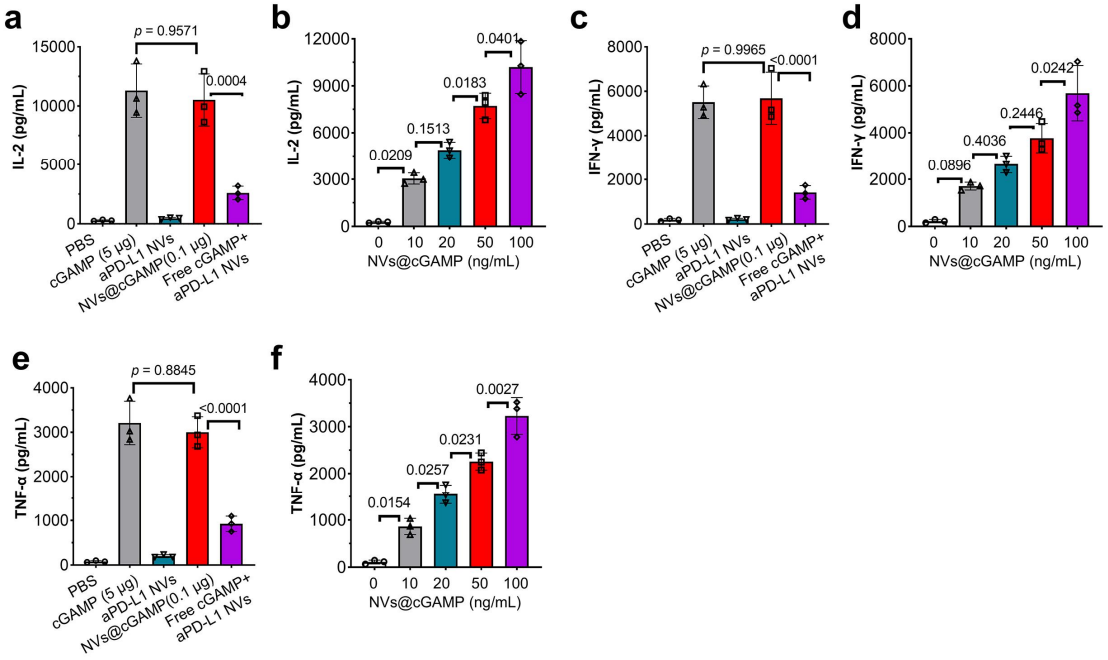

Supplementary Figure 12. Effect of agents on cytokine secretion during CAR-T killing of tumor cells. (a, c and e) IL-2, IFN-γ and TNF-α levels in the supernatants after 12 h of addition of different agents to the co-incubation system of CAR-T cells, DCs and LLC-MSLN cells were assessed by ELISA (n = 3 independent experiments). (b, d and f) After adding different doses of aPD-L1 NVs@cGAMP to the co-incubation system of CAR-T cells, DCs and LLC-MSLN cells for 12 h, the dose-dependent release of IL-2, IFN-γ and TNF-α was detected by ELISA (n = 3 independent experiments). The p values were determined by one-way ANOVA with Tukey's post-test for (a), (c) and (e). Source data underlying a–f are provided as a Source Data file.

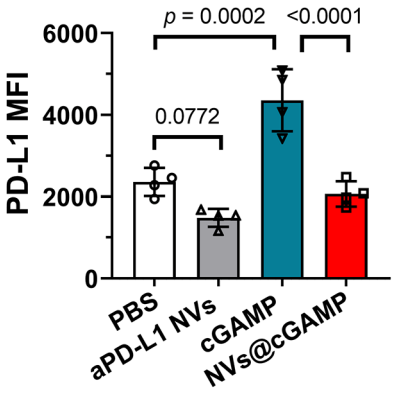

Supplementary Figure 13. Blockade of PD-L1 by NVs@cGAMP. After treatment of LLC-MSLN tumor-bearing mice with PBS, cGAMP, aPD-L1 NVs and NVs@cGAMP, tumor tissues were isolated and PD-L1 expression on the surface of tumor cells was detected by flow cytometry (n = 4 mice). Data are expressed as mean ± S.D. The p values were determined by one-way ANOVA with Tukey's post-test. Source data are provided as a Source Data file.

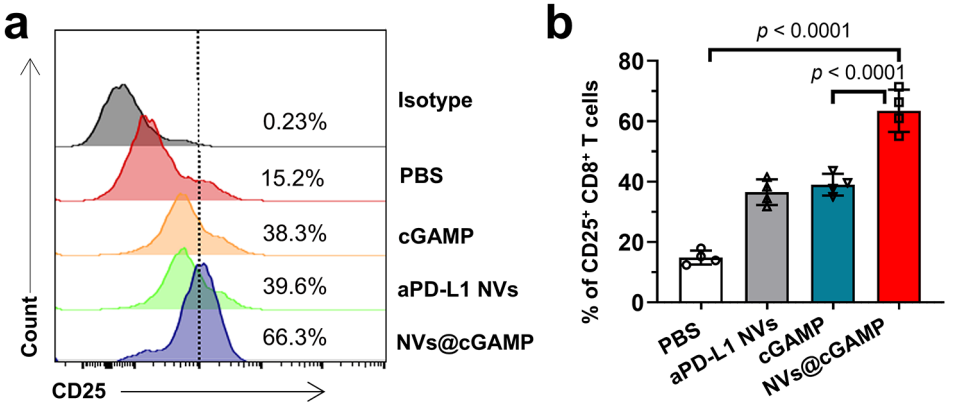

Supplementary Figure 14. CD25 expression levels on T cells. Representative flow cytometry plots and statistical analysis of CD25 expression levels on T cells across different treatment groups by flow cytometry (n = 4 mice). The p values were determined by one-way ANOVA with Tukey's post-test. Source data underlying b are provided as a Source Data file.

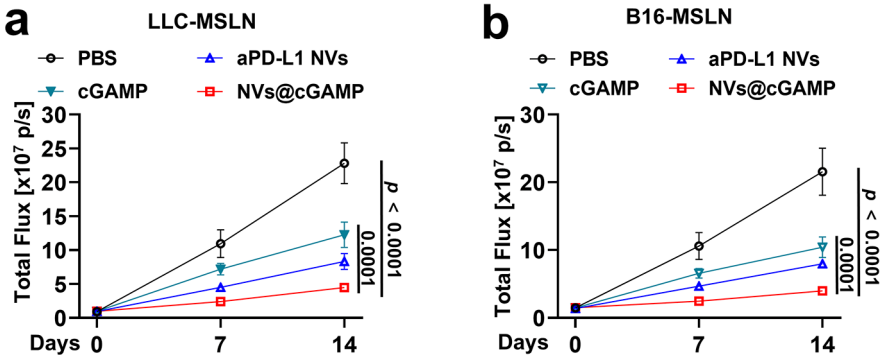

Supplementary Figure 15. Statistical analysis of bioluminescence intensity. (a-b) Bioluminescence intensity was measured in (a) LLC-MSLN tumor-bearing mice and (b) B16-MSLN tumor-bearing mice after receiving various treatments, followed by statistical analysis (n = 4 mice). Data are expressed as mean ± S.D. The p values were determined by two-way ANOVA with Tukey's post-test. Source data underlying a–b are provided as a Source Data file.

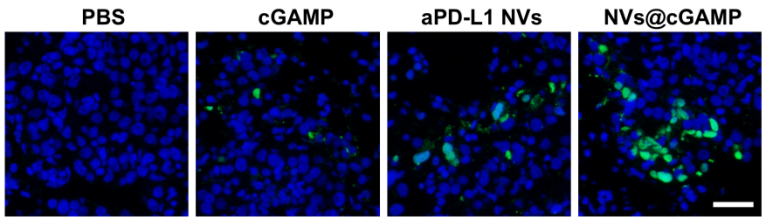

Supplementary Figure 16. TUNEL staining of lung tumor tissue sections. Lung tumor tissue damage was assessed by TUNEL staining after various treatments in tumor-bearing mice. Experiment was repeated three times independently with similar results. Scale bar: 100 μm.

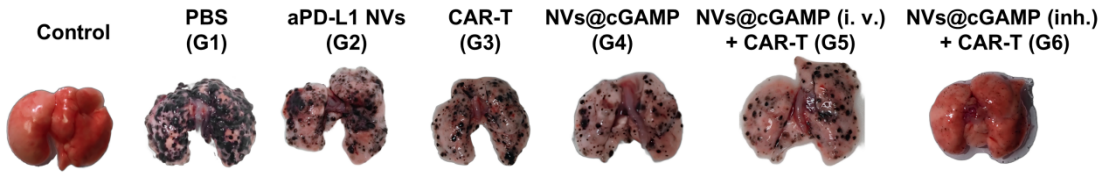

Supplementary Figure 17. Lung metastases in tumor-bearing mice. Representative images of the lungs of B16-MSLN tumor-bearing mice from the different treatment groups (n = 4 mice).

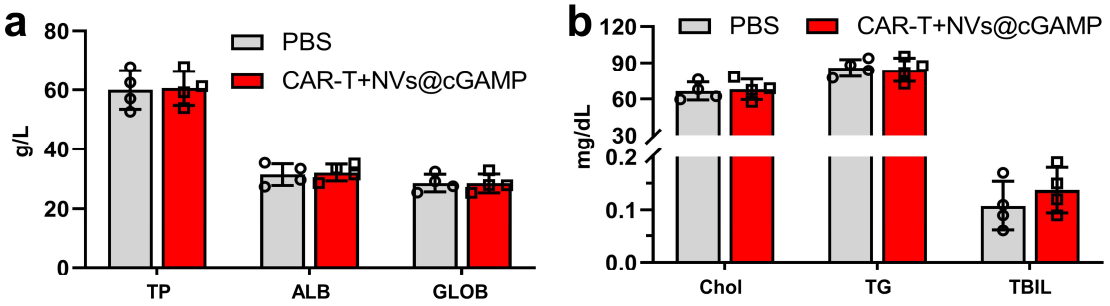

Supplementary Figure 18. Safety assessment of combination therapy. After mice received PBS or combination therapy, mouse serum was collected for biochemical analysis to assess the safety of combination therapy (n = 4 mice). Total Protein (TP), Albumin (ALB), Globulin (GLOB), Cholesterol (CHOL), Triglycerides (TG), Total Bilirubin (TBIL). All data are presented as the mean ± S.D. Source data underlying a–b are provided as a Source Data file.

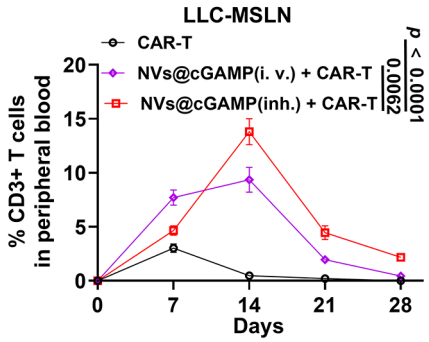

Supplementary Figure 19. Percentage of CAR-T cells in the peripheral blood of tumor-bearing mice. The percentage of CAR-T cells in peripheral blood at various time points after injection of GFP-expressing MOCK-T or MSLN CAR-T cells into LLC-MSLN tumor-bearing mice (n = 4 mice). Data are expressed as mean ± S.D. The p values were determined by two-way ANOVA with Tukey's post-test. Source data are provided as a Source Data file.

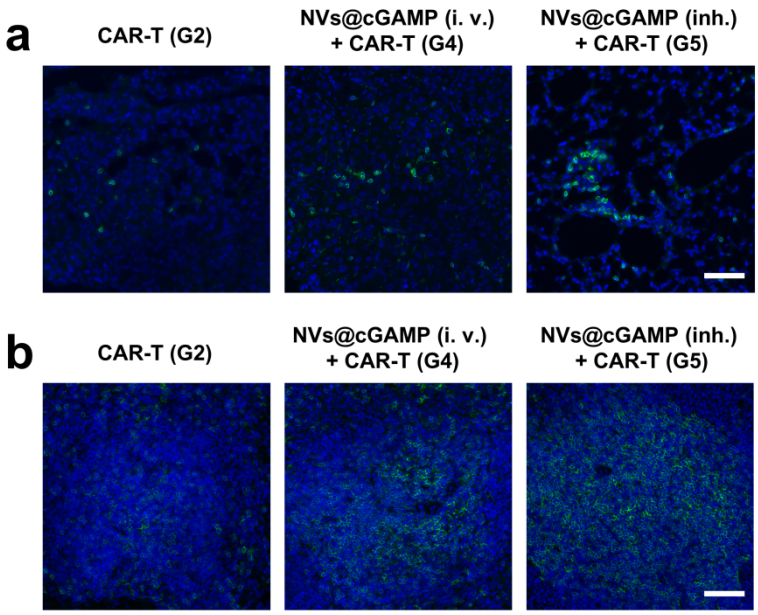

Supplementary Figure 20. Infiltration of CAR-T cells in tissues. (a) After different treatments were administered to LLC-MSLN tumor-bearing mice, CAR-T cell infiltration in tumor tissues was observed using confocal microscopy. Scale bar: 50 μm. (b) After different treatments were administered to LLC-MSLN tumor-bearing mice, CAR-T cell infiltration in spleens was observed using confocal microscopy. Experiment was repeated three times independently with similar results. Scale bar: 100 μm.

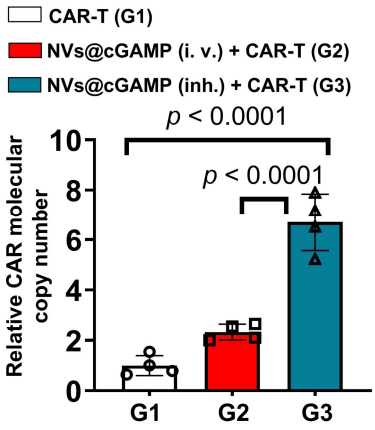

Supplementary Figure 21. Proliferation of CAR-T cells in tumor tissue. The copy number of CAR per microgram of genomic DNA was assessed by qPCR to evaluate intratumoral CAR-T cell proliferation ($n = 4$ mice). All data are presented as the mean ± S.D. The p values were determined by one-way ANOVA with Tukey's post-test. Source data are provided as a Source Data file.

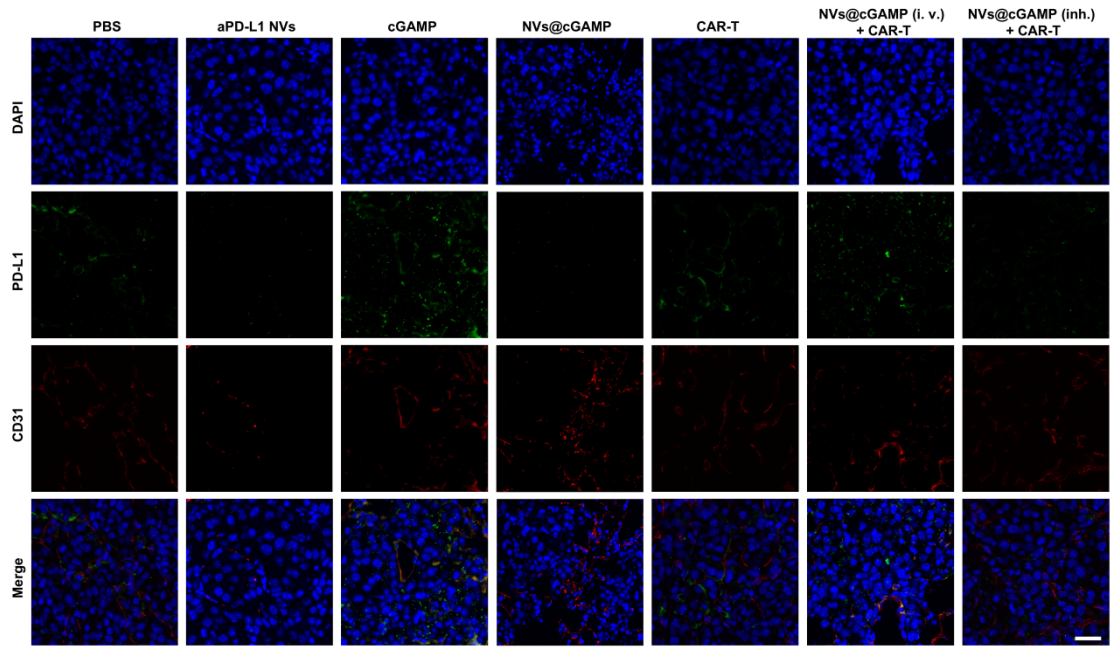

Supplementary Figure 22. Co-expression of CD31 and PD-L1 in tumor tissues. Following different treatments of LLC-MSLN tumor-bearing mice, co-expression of CD31 (red) and PD-L1 (green) in tumor tissues was analyzed by confocal microscopy, with CD31 serving as a vascular marker. Experiment was repeated three times independently with similar results. Scale bar: 50 μm.

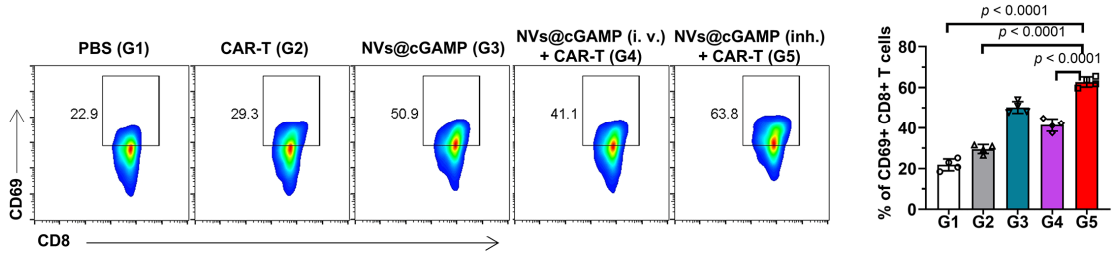

Supplementary Figure 23. CD69 expression levels on CD8$^+$ T cells. Representative flow cytometry plots and statistical analysis of CD69 expression on T cells within the TME across various treatment groups (n = 4 mice). Data are presented as the mean ± S.D. The p values were determined by one-way ANOVA with Tukey's post-test. Source data underlying b are provided as a Source Data file.

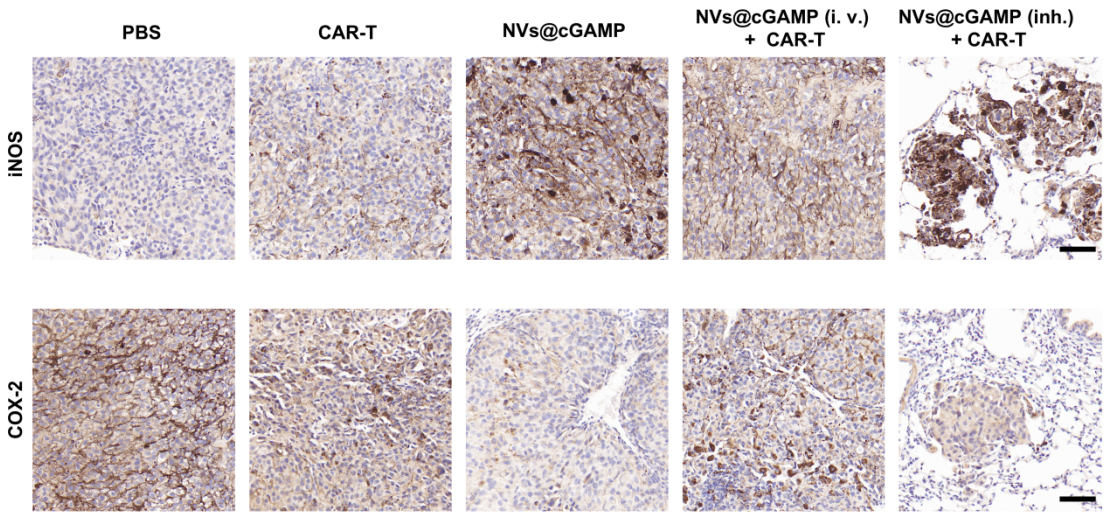

Supplementary Figure 24. Expression of iNOS and COX-2. LLC-MSLN tumor-bearing mice receiving different treatments were assessed for iNOS and COX-2 expression in tumor tissues via immunohistochemistry. Experiment was repeated three times independently with similar results. Scale bar: 200 μm.

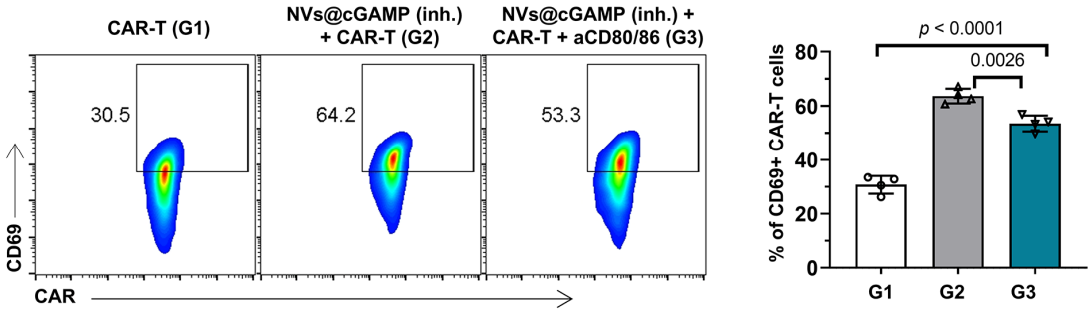

Supplementary Figure 25. CD69 expression levels on CAR-T cells. Representative flow cytometry plots and statistical analysis of CD69 expression on CAR-T cells in peripheral blood across various treatment groups (n = 4 mice). Data are presented as the mean ± S.D. The p values were determined by one-way ANOVA with Tukey's post-test. Source data underlying b are provided as a Source Data file.

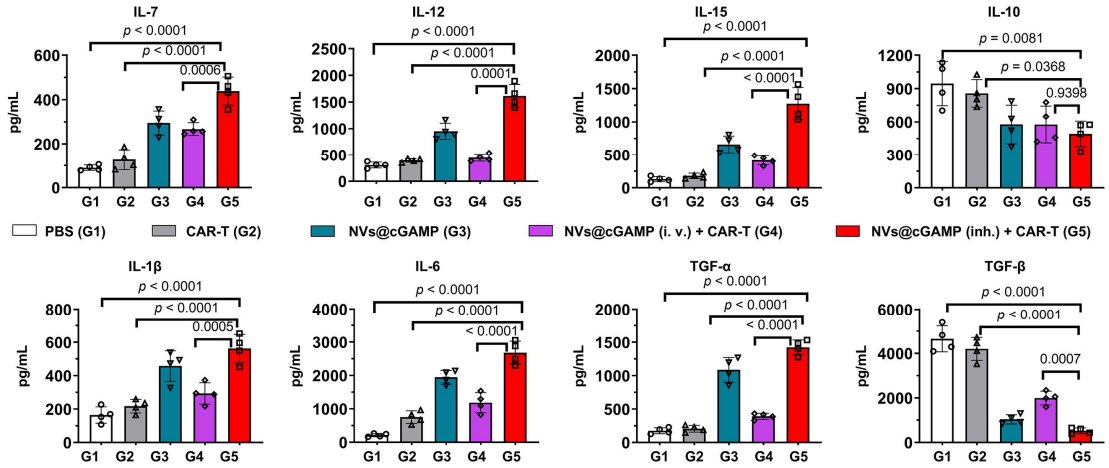

Supplementary Figure 26. Quantification of cytokines in tumor tissues. Cytokine concentrations of IL-7, IL-12, IL-15, IL-10, IL-1β, IL-6, TGF-α and TGF-β in tumor tissue homogenates from different treatment groups were quantified by ELISA (n = 4 mice). Data are presented as the mean ± S.D. The p values were determined by one-way ANOVA with Tukey's post-test. Source data are provided as a Source Data file.

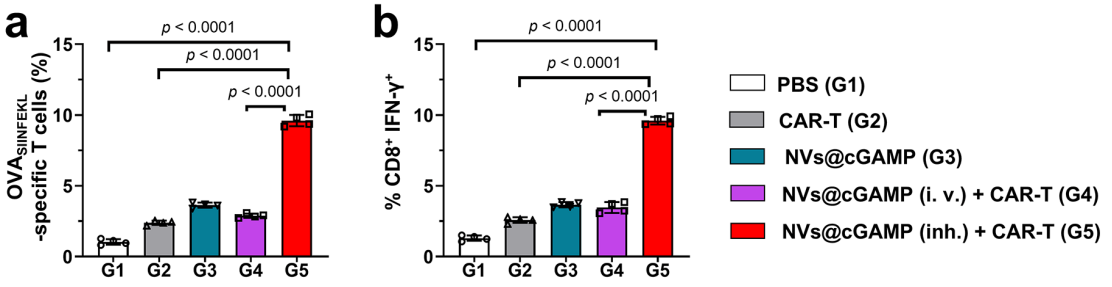

Supplementary Figure 27. Assessment of epitope spreading. (a) In LLC-MSLN-OVA tumor-bearing mice, the percentage of OVA $_{(SIINFEKL)}$-specific $CD8^+$ T cells in the spleen was assessed *via* flow cytometry after various treatments (n = 4 mice). (b) Following stimulation with OVA peptides, the percentage of T cells producing IFN-γ within the $CD8^+$ T cell population was analyzed across different treatment groups (n = 4 mice). Data are presented as the mean ± S.D. The p values were determined by one-way ANOVA with Tukey's post-test for (a) and (b). Source data underlying a–b are provided as a Source Data file.

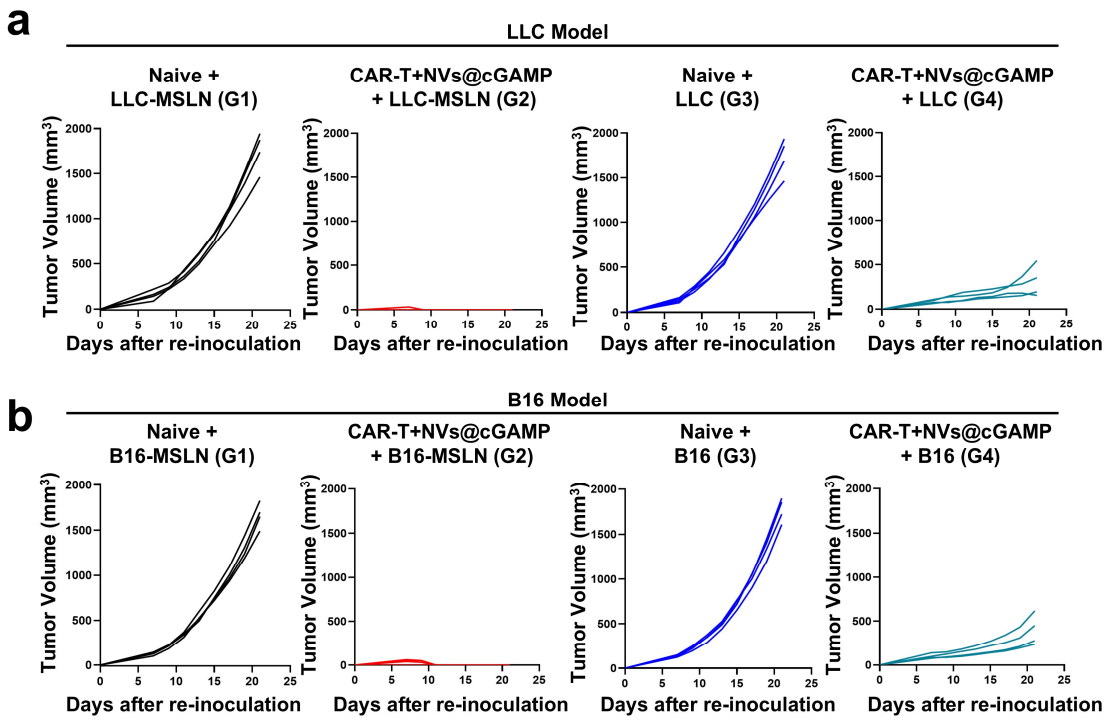

Supplementary Figure 28. Changes in tumor volume in tumor-bearing mice. (a) In the LLC tumor relapse model, tumor volume changes were assessed in naive mice and mice cured by combination therapy after subcutaneous inoculation of LLC or LLC-MSLN cells (n = 4 mice). (b) In the B16 tumor relapse model, tumor volume changes were assessed in naive mice and mice cured by combination therapy after subcutaneous inoculation of B16 or B16-MSLN cells (n = 4 mice). Source data underlying a–b are provided as a Source Data file.

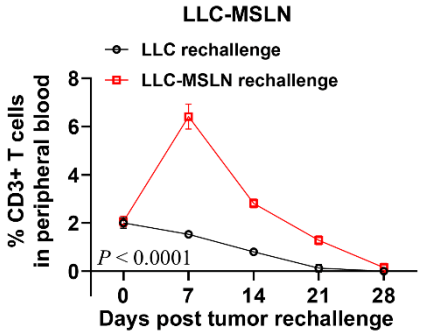

Supplementary Figure 29. Percentage of CAR-T cells in the peripheral blood of tumor-bearing mice. The percentage of CAR-T cells in peripheral blood at various time points after cured mice were rechallenged with either mesothelin (MSLN)-overexpressing tumor cells or parental cells (n = 4 mice). Data are presented as the mean ± S.D. The p values were determined by two-way ANOVA with Tukey's post-test. Source data are provided as a Source Data file.

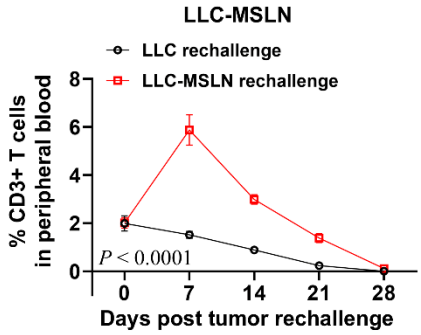

Supplementary Figure 30. Percentage of CAR-T cells in the peripheral blood of tumor-bearing mice. Following subcutaneous injection of MSLN-overexpressing tumor cells or parental cells into the inguinal region of cured mice, the percentages of CAR-T cells in the peripheral blood of LLC-MSLN tumor-bearing mice were analyzed over time ($n = 4$ mice). Data are presented as the mean ± S.D. The p values were determined by two-way ANOVA with Tukey's post-test. Source data are provided as a Source Data file.

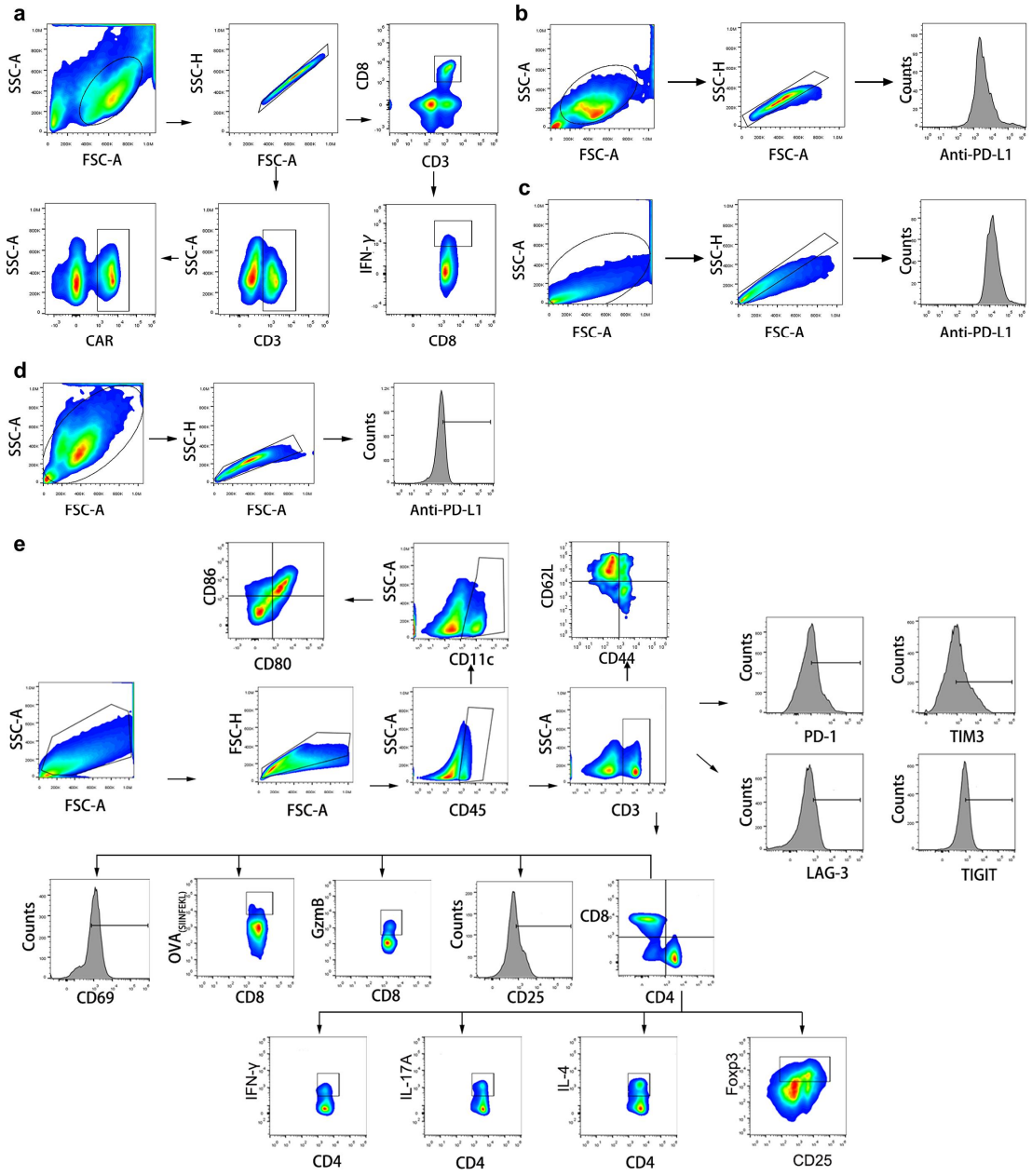

Supplementary Figure 31. Gating strategy for flow cytometry. a. Representative gating strategies shown for CAR-T (Fig. 1c) and IFN-γ–producing $CD8^+$ T cells (Fig. 8d). b-c. Expression of the anti-PD-L1 scFv on aPD-L1 293T cells (Fig. 3b) and aPD-L1 NVs (Fig. 3f). d. PD-L1 blockade on the PC-9 cell (Fig. 3g). e. $CD8^+$ T cells and $CD4^+$ T cells (Fig. 5b, Fig. 7b), Treg cells (Fig. 5c, Fig. 7h) , MDSCs (Fig. 5e, Fig. 7h), Th cells (Fig. 5g), memory T cells (Fig. 5j), granzyme B-expressing $CD8^+$ T cells (Fig. 7c), mature DCs (Fig. 7h) within the TME, exhaustion markers on T cells (Fig. 5e), CD25 (Supplementary Fig. 14) and CD69 (Supplementary Fig. 23) expression on CD8+ T cells, and $OVA_{(SIINFEKL)}$-specific $CD8^+$ T cells (Fig. 8c).

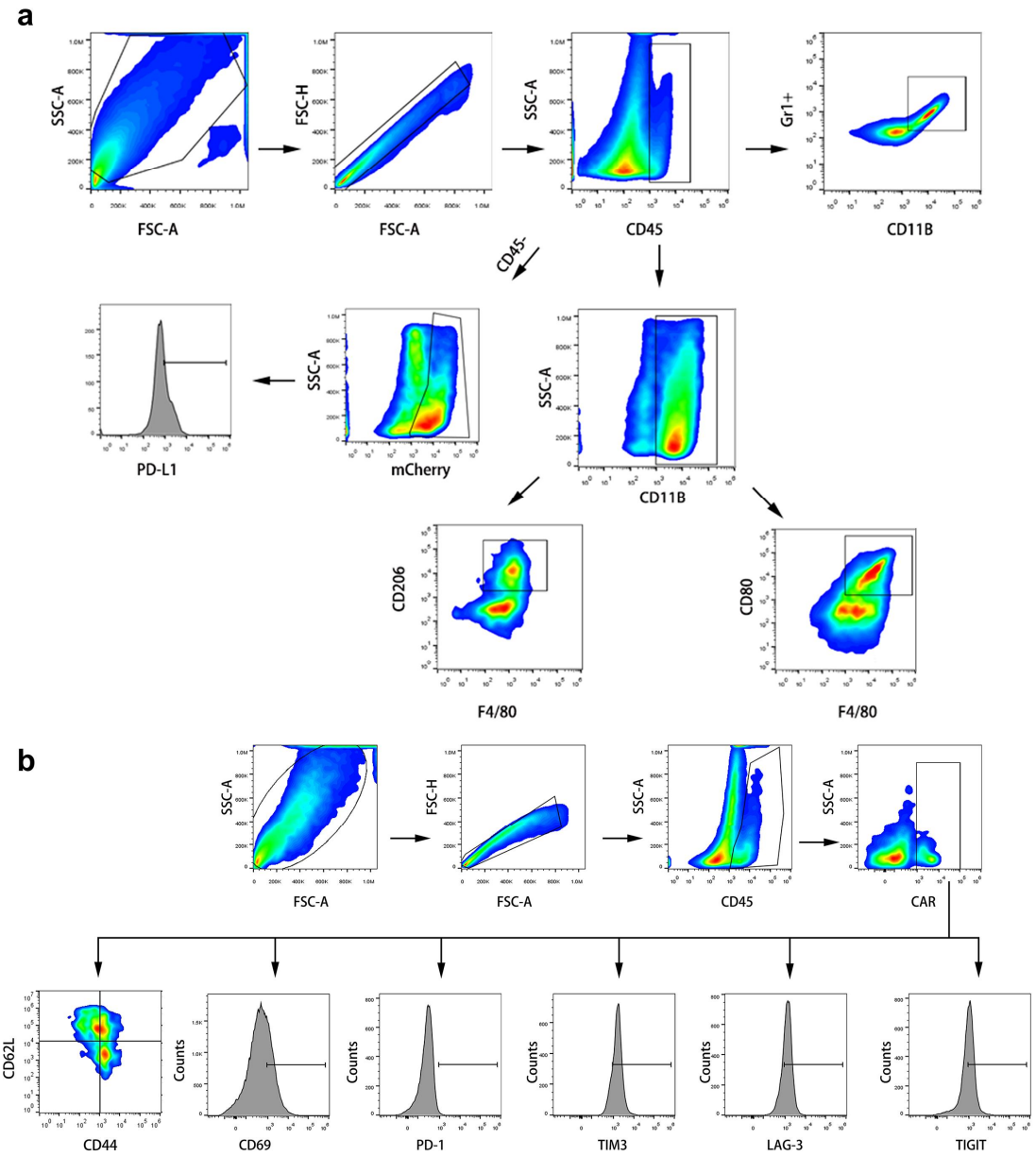

Supplementary Figure 32. Gating strategy for flow cytometry. a. Representative gating strategies shown for MDSCs (Fig. 5d) macrophages (Fig. 7g) within the TME and PD-L1 expression on tumor cells (Supplementary Fig. 13). b. Exhaustion markers on CAR-T cells (Fig. 7d), memory T cells within the CAR-T cell population (Fig. 7i) and CD69 expression on CAR-T cells (Supplementary Fig. 25).

Supplementary Table 1. Primers used for current study

Gene name	Forward 5'-3'	Reverse 5'-3'
Anti-MSLN CAR	TCTGGAGTGGCTGGGAGTAATATGG	TTGGCTCTTGGAGTTGTCCTTGATG
U6	CTCGCTTCGGCAGCACAT	TTTGCGTGTCATCCTTGCG
Mouse IFN-γ	CAGCAACAGCAAGGCGAAAAAGG	TTTCCGCTTCCTGAGGCTGGAT
Mouse CXCL-9	CCTAGTGATAAGGAATGCACGATG	CTAGGCAGGTTTGATCTCCGTTC
Mouse CXCL-10	ATCATCCCTGCGAGCCTATCCT	GACCTTTTTTGGCTAAACGCTTTC

Mouse IFN-β	GCCTTTGCCATCCAAGAGATGC	ACACTGTCTGCTGGTGGAGTTC
Mouse CD274	TGCGGACTACAAGCGAATCACG	CTCAGCTTCTGGATAACCCTCG
Mouse GAPDA	CATCACTGCCACCCAGAAGACTG	ATGCCAGTGAGCTTCCCGTTCAG
Mouse IFIT1	TACAGGCTGGAGTGTGCTGAGA	CTCCACTTTCAGAGCCTTCGCA
Mouse IFIT2	CGAACTACCGTCTGGATGACTG	CTTCAACCAGCGCCATTGCTTG
Mouse ISG15	CATCCTGGTGAGGAACGAAAGG	CTCAGCCAGAACTGGTCTTCGT

209